ACS ES&T Water

pubs.acs.org/estwater

Article

Water Treatment Method for Removal of Select Heavy Metals and Nutrient Ions Through Adsorption by Magnetite

Teagan J. Leitzke,* J. Downey, Richard M. LaDouceur, Daisy M. Margrave, Grant C. Wallace, and David L. Hutchins

Cite This: *ACS EST Water* 2022, 2, 1584−1592

Read Online

ACCESS | Metrics & More | Article Recommendations | Supporting Information

ABSTRACT: This study explored the removal of contaminants from surrogate solutions using magnetite particles. Commercially available magnetite was used for the removal of copper, lead, nitrate, and phosphate from surrogate solutions. Single-stage experiments with copper, lead, and phosphate surrogate solutions achieved over 98% removal, while nitrate removal experiments only achieved 7.47%, in 24 h at high (20 g/L) magnetite doses and initial concentrations of 100 mg contaminant/L. Two-stage experiments with copper showed over 99.9% cumulative removal after the second stage. Adsorption kinetics experiments for copper, lead, and phosphate demonstrate rapid uptake of contaminants with high doses of magnetite, removing over 90% of contaminants in 4 min or less and follow a pseudo-second-order model. Ultimately, this study aims to establish the minimum magnetite dose and/or minimum number of stages required to remove contaminants below water quality standards for human and/or aquatic life. Water pollution is a serious global issue, and this study poses a potential solution that can be modified for a variety of applications, including environmental contamination and industrial wastewater treatment.

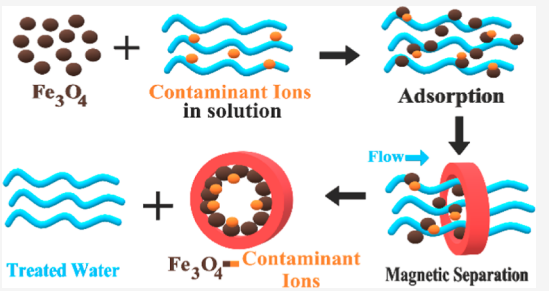

KEYWORDS: *magnetite, adsorption, kinetics, contaminant removal, copper*

1. INTRODUCTION

Natural water sources and industrial wastewaters can contain trace levels of harmful contaminants, such as heavy metals and nutrients. Though not clearly defined, heavy metals are metals and metalloids with high densities that are toxic at low-level exposure.[1−3] Heavy metals exposure can occur due to natural phenomenon, such as weathering, and anthropogenic activities, including municipal wastewater release, industrial operations, and mining.[1−9] Nutrient contamination can come from anthropogenic sources, including food product processing and agricultural runoff, and geogenic activity.[6,10−13] Exposure to these toxic materials can lead to adverse health effects in humans and the environment.

Heavy metals, such as arsenic and copper, are known to be toxic and, at elevated levels, can lead to organ damage, cancer, and respiratory problems in humans. Plant life can also be affected by heavy metals, causing cell damage and nutrient deficiency.[1,2,6,7,14] Copper is of interest because it accumulates in the organs of fish, leading to developmental or respiratory problems.[4,15] Aquatic species are highly sensitive to contaminants, and local fish kills tend to be caused by heavy rain and flooding that deposit metals from contaminated areas into streams and tributaries, where copper is highly prominent.[16] Nutrients, such as nitrates and phosphates, can also have toxic effects at increased concentrations.[17,18] Nitrates and phosphates can cause cancer, organ damage, and immune system changes in humans. Affected waters could experience eutrophication, where dissolved oxygen depletion causes problems for aquatic life and can produce harmful algal blooms.[12,19−21] Even at low concentrations, below 3 μg/L, contaminants can be harmful, and their removal and recovery at these levels can be difficult.[17,18,22]

The release and improper care of contaminated wastewaters pose serious threats to the environment, aquatic life, and human health, and the need for an efficient and economical method for contaminant removal is apparent. Researchers are currently exploring various methods to address contaminant removal, including ion exchange, biochar, reverse osmosis, adsorption, and a selective capacitive removal technology employing electro-adsorption or capacitive deionization.[7,10,12,19,23,24] This work examined the adsorption method, using magnetite (Fe_3O_4) particles as the adsorbent. Adsorption is efficient, simple, and produces less byproducts than methods such as membrane filtration, ion exchange, and chemical precipitation.[5,7,25,26] Fe_3O_4 is inexpensive, already exists in the

Received: May 26, 2022
Revised: July 28, 2022
Accepted: July 29, 2022
Published: August 15, 2022

https://doi.org/10.1021/acsestwater.2c00242
ACS EST Water 2022, 2, 1584−1592

environment, and has several favorable characteristics including biocompatibility, magnetic susceptibility, and an easily modified surface.[5,7,8,25,27−31] Magnetic properties allow for easy and efficient collection, reducing chemicals needed for removal and decreasing the production of secondary pollutants.[26,34,35] Additionally, Fe_3O_4 can effectively capture anions and cations across a range of pH values.[13,26,27,32,33] Further, Fe_3O_4 has demonstrated potential in applications such as magnetic inks, MRI contrast agents, and water treatment.[27−31]

This work used Fe_3O_4 in a series of experiments designed to explore its adsorption properties for the removal of heavy metal and nutrient ions from surrogate solutions. Experiments included investigation of loading capacity, kinetics, single- and two-stage removal, and cycling. A model was also generated and validated using Design-Expert 12, a logistic regression analysis software. Fe_3O_4 was the focus of in-depth experimentation due to its cost, environmental friendliness, and natural adsorptive properties for contaminant removal, specifically for use in a novel continuous flow material recovery (CFMR) system designed for water treatment.[27,29,36] Environmental and industrial applications, including treating contaminated tributaries and industrial waste streams, are highly desirable applications for this work.

2. MATERIALS

Commercially available Fe_3O_4 was purchased from SkySpring Nanomaterials (Fe_3O_4, 98 + %, 20−30 nm) and, for comparison, from U.S. Research Nanomaterials (Fe_3O_4, 98 + %, 20−30 nm). Scanning electron microscope (SEM) images can be found in the Supporting Information Text S1 and Figure S1. All experiments in this work used Fe_3O_4 from SkySpring Nanomaterials.

Surrogate solutions were prepared using one of the following chemical compounds. Copper(II) sulfate pentahydrate purchased from Sigma-Aldrich; lead(II) acetate trihydrate, calcium nitrate, and methanol purchased from Fisher Scientific; and lead(II) nitrate and potassium phosphate dibasic purchased from J.T. Baker Chemical Co. Copper inductively coupled plasma (ICP) standards were purchased from Ricca Chemical and Sigma-Aldrich.

3. EXPERIMENTAL METHODS

3.1. Kinetics. Kinetics experiments were performed to determine the adsorption rate of contaminants onto Fe_3O_4. Copper sulfate pentahydrate, lead acetate, or potassium phosphate dibasic was used to prepare the solutions. Experiments were conducted using a known starting contaminant concentration and a dose of 10 or 20 g Fe_3O_4 in 1 L of 18 MΩ deionized (DI) water, agitated at 400 or 600 rpm. The contaminant concentration and pH were monitored and recorded at specified sampling times over the course of 6 h. All experiments were conducted at intrinsic pH, room temperature, and ambient pressure. All samples were analyzed by a Hach DR3900 spectrophotometer.

3.2. Contaminant Removal Experiments. *3.2.1. Loading Experiments.* The protocol for evaluating Fe_3O_4 loading is as follows.[36] Fe_3O_4 was weighed and poured into a flask, followed by methanol to wet the particles. 18 MΩ DI water was added to the flask and sonicated under vacuum. In a separate beaker, a contaminant ion solution was prepared with 18 MΩ DI water and then added to the flask with the Fe_3O_4 slurry for a total volume of 250 mL. Finally, the flask was placed on a shaker table for 24 h, assuming equilibrium loading was achieved by this time. At 24 h, a sample was taken and immediately filtered and analyzed. All experiments were conducted at intrinsic pH, room temperature, and ambient pressure, and all samples were analyzed by a Hach DR3900 spectrophotometer. The dose of particles and contaminant concentration were adjusted to the desired values for each experiment. The total volume, 250 mL, was chosen based on convenience and for comparison to prior testing.[36]

From these data, loading and removal efficiency can be calculated. Loading was calculated according to eq 1

$$q = \frac{(C_0 - C_e)V}{m} \tag{1}$$

where q is the loading capacity (mg/g), C_0 and C_e are the initial and final concentrations (mg/L), respectively, V is the total volume of the solution (L), and m is the mass of the adsorbent (g).[37] Loading describes how much contaminant can be removed from a system per gram of adsorbent added to the system. The removal efficiency is given by eq 2

$$\%\ \text{Removal} = \frac{(C_0 - C_e)}{C_0} \times 100 \tag{2}$$

where C_0 and C_e are defined in the same manner as in eq 1.[37] Removal efficiency expresses the percentage of contaminant removed from the system by comparing the initial and final contaminant concentrations.

3.2.2. Single- and Two-Stage Experiments. Single-stage contaminant ion removal experiments were performed for a variety of single and mixed contaminant surrogate solutions. To demonstrate that complete, or near-complete, removal is possible with an increased number of particles, the dose for these experiments was increased to 20.0 g Fe_3O_4/L. Copper sulfate pentahydrate, lead acetate, potassium phosphate dibasic, or calcium nitrate were used to make single contaminant solutions. Mixed contaminant solutions were prepared using either lead nitrate for a solution containing lead and nitrate ions or copper sulfate pentahydrate and lead acetate for a solution containing copper and lead ions. Mixed contaminant experiments were conducted to determine Fe_3O_4 performance in the presence of competing ions and loading of the respective ions relative to each other.

The procedure for single-stage removal is as follows. In a 1 L beaker, 100 mg of contaminant/L was completely dissolved in 250 mL of 18 MΩ DI water, and the initial pH of the contaminant solution was measured. The beaker was then placed under mechanical agitation, mixing at 400 rpm. Fe_3O_4 was weighed and added to the contaminant solution. After 1 h of mixing, the pH was measured and a sample was taken. Samples were immediately filtered and analyzed using a Hach DR3900 spectrophotometer. All experiments were conducted at intrinsic pH, room temperature, and ambient pressure. For comparison to loading and kinetics experiments, the initial contaminant concentration was kept at approximately 100 mg/L for all experiments with two exceptions. First, the PO_4^{3-} concentration was increased because the initial 100 mg/L experiment produced results below the specified detection limit of the Hach TNT845 vials. Second, Pb(II) concentrations were maintained approximately at the baseline for single and Cu(II) mixed experiments; however, for the NO_3^- mixed experiment, it was decided to keep the NO_3^-

https://doi.org/10.1021/acsestwater.2c00242
ACS EST Water 2022, 2, 1584−1592

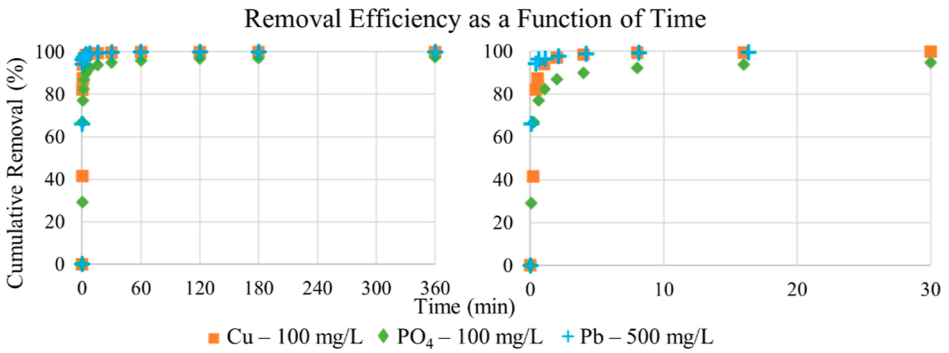

Figure 1. Removal efficiencies over a 6 h period (left) and a 30 min snapshot of the data (right). Copper (squares), phosphate (diamonds), and lead (pluses) removal with 20 g Fe_3O_4/L in solution, agitated at 400 rpm.

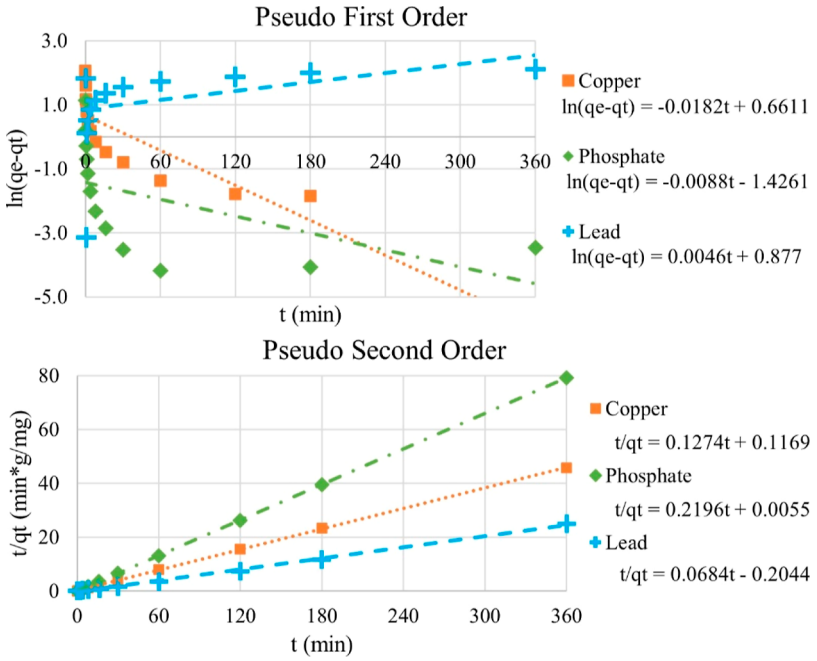

Figure 2. PFO (top) and PSO (bottom) kinetic models fitted to the experimental data for copper (squares), phosphate (diamonds), and lead (pluses) removal by Fe_3O_4 particles. Trend lines are linear fits to the data, and the equations are presented at the right on both graphs.

concentration at the baseline, so the Pb(II) concentration was elevated due to the stoichiometric Pb to NO_3^- ratio in the lead nitrate powder used to prepare the solution.

Two-stage contaminant ion removal experiments were conducted for surrogate Cu(II) solutions. The procedure for two-stage removal is the same as the procedure described in the previous paragraph with the addition of the second stage, which is as follows. After the first hour of mixing, the pH was measured and a 40 mL sample was taken, filtered, and preserved to under pH 2 using nitric acid. A magnet was used to separate Fe_3O_4 from the depleted Cu(II) solution, which was decanted into another 1 L beaker. The beaker was placed back under mechanical agitation at 400 rpm, and a fresh mass of Fe_3O_4 was added to the solution and mixed for another hour. After the second hour, another 40 mL sample was taken, filtered, and preserved to under pH 2 using nitric acid. All experiments were conducted at intrinsic pH, room temperature, and ambient pressure. Samples were analyzed using an iCAP 6500 Series inductively coupled plasma-optical emission spectrometer (ICP-OES).

3.3. Cycling. Cycling was of interest in an economic aspect, where particle reusability would decrease the need to constantly purchase new adsorbent material and minimize disposal products. Two cycling experiments using copper(II) sulfate pentahydrate were conducted, with each cycle being run the same as a 24 h loading experiment, as described in Section 3.2.1. One experiment consisted of adding fresh Fe_3O_4 to the Cu(II) solution after each cycle and the other added stripped and regenerated Fe_3O_4. Each experiment cycled their respective solutions until essentially all Cu(II) was removed. A 2 mL sample was taken after each cycle and immediately filtered and analyzed. All tests were performed at intrinsic pH, room temperature, and ambient pressure. All samples were analyzed using a Hach DR3900 spectrophotometer.

The strip and regeneration processes for Cu(II)-loaded Fe_3O_4 is as follows. Particles were stripped in a sulfuric acid solution at pH 1.4. The solution was mixed for 3 min, then the particles were magnetically separated from the solution. The strip solution pH was recorded, a sample of at least 15 mL was taken, and the rest was decanted into a waste container. Two wash steps followed, where DI water was mixed with the particles for 3 min, then the particles were separated, and a solution sample taken. Regeneration was performed in the same manner as the strip, except that an ammonium hydroxide

https://doi.org/10.1021/acsestwater.2c00242
ACS EST Water 2022, 2, 1584−1592

Table 1. Kinetic Model Parameters

		PFO kinetic model			PSO kinetic model		
	q_e(exp) (mg/g)	k_1(1/min)	q_e(mg/g)	R^2	k_2(g/mg·min)	q_e(mg/g)	R^2
Cu(II)	7.87	0.018	1.94	0.64	0.14	8.55	0.99
PO_4^{3-}	4.55	0.009	0.52	0.68	8.77	4.55	1
Pb(II)	14.47	−0.005	2.40	0.10	−0.02	14.62	0.99

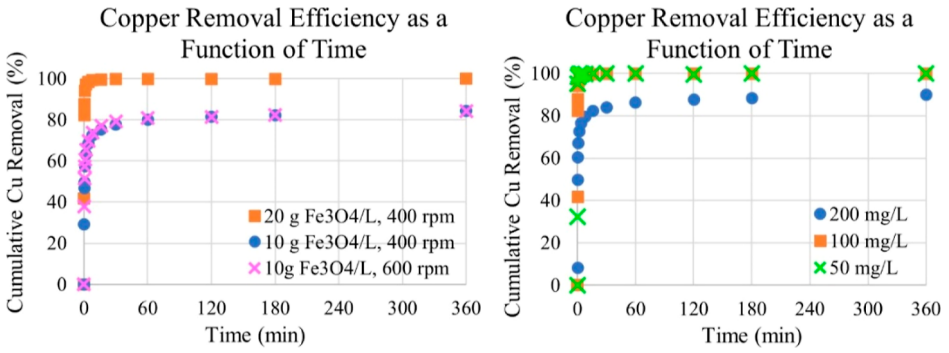

Figure 3. Removal efficiencies of copper over 6 h. Left: doses of 20 g/L (squares) and 10 g/L (circles, X's) Fe_3O_4 with an approximately constant initial concentration of 100 mg Cu(II)/L and agitation speeds of 400 rpm (squares, circles) and 600 rpm (X's) were used. Right: 200 mg (circles), 100 mg (squares), and 50 mg (X's) of copper per liter with 20 g Fe_3O_4/L in solution, agitated at 400 rpm.

solution at pH 11.46 was used instead of sulfuric acid.[36] Stripping and regenerating the particles is beneficial for economic considerations, as it serves a dual purpose: to recycle and reuse particles in the CFMR system and to recover metal by using the strip solution in an electrowinning cell.

3.4. Design of Experiments. Design-Expert 12 was used to develop a statistical design of experiments to determine optimal conditions for Cu(II) adsorption onto Fe_3O_4. A series of 13 experiments, augmented with two additional experiments were conducted to determine the effects of pH and Fe_3O_4 dose on adsorption. The adsorbent dose and pH were varied from 6 to 20 g Fe_3O_4/L and from 2 to 4.5, respectively, while the initial Cu(II) concentration was approximately 80 mg/L. Solutions were prepared by adding copper(II) sulfate pentahydrate to 18 MΩ DI water and then adjusting the pH with sulfuric acid. Fe_3O_4 was added to the solution and left to mechanically agitate at 400 rpm for 1 h to ensure maximum adsorption was attained, after which samples were immediately filtered and analyzed. All experiments were conducted at room temperature and ambient pressure, and all samples were analyzed by a Hach DR3900 spectrophotometer. Results were used by Design-Expert 12 to generate a response surface model and determine optimal parameters.

4. RESULTS AND DISCUSSION

4.1. Kinetics. Cu(II), PO_4^{3-}, and Pb(II) were used in kinetics experiments to determine their adsorption rate onto Fe_3O_4 and which kinetic model the adsorption followed. Experiments were conducted over 6 h, using a dose of 20 g Fe_3O_4/L and an agitation speed of 400 rpm, with initial concentrations of 100 mg/L for Cu(II) and PO_4^{3-} and 500 mg/L for Pb(II). The Pb(II) concentration was increased because the 100 mg/L experiment resulted in concentrations below the detection limit of the spectrophotometer within 30 s. Figure 1 exhibits cumulative removal over time for each experiment, where initial adsorption occurs quickly due to many available adsorption sites, and, as time passes, it gradually decreases due to limited availability of adsorption sites and contaminant contact with available sites. Cu(II) removal, squares in Figure 1, reached 90% within 1 min and 99% within 8 min of contact with Fe_3O_4. Pb(II), pluses in Figure 1, shows similar removal with 96% removal in 1 min and 99% in 8 min. PO_4^{3-}, diamonds in Figure 1, has slightly slower adsorption, achieving over 90% removal in 4 min and an overall removal of approximately 98%.

To evaluate adsorption kinetics, pseudo-first-order (PFO) and pseudo-second-order (PSO) kinetic models were fit to the experimental data, visually presented in Figure 2 and quantitatively described in Table 1. PFO and PSO kinetics are expressed by eqs 3 and 4, respectively,

$$\ln(q_e - q_t) = \ln(q_e) - k_1 t \tag{3}$$

$$\frac{t}{q_t} = \frac{t}{q_e} + \frac{1}{k_2 \times q_e^2} \tag{4}$$

where q_e is the equilibrium loading capacity, q_t is the loading capacity at time t, and k_1 and k_2 are the adsorption rate constants for the PFO and PSO models, respectively.[38]

Kinetic parameters are given in Table 1, where q_e (exp) is the experimental value for loading equilibrium and R^2 is the correlation coefficient, which describes the statistical relevance between two variables. Comparing the models, the R^2 values indicate a better fit to the PSO model in all cases, with values at or above 0.99, whereas the PFO R^2 values are less than 0.7 in all cases. Comparing q_e to q_e (exp) for the models reveals a better fit to the PSO model, indicating that it is better suited to describe the adsorption kinetics for Cu(II), PO_4^{3-}, and Pb(II) onto Fe_3O_4. The PSO model suggests that the rate-limiting step is controlled by chemical adsorption and the surface interactions of the contaminants and Fe_3O_4 functional groups.[38−40]

In addition to different contaminants, the agitation speed and dose were varied, maintaining solution concentrations at 100 mg Cu(II)/L, presented at left in Figure 3. At 20 g Fe_3O_4/L concentration and 400 rpm speed, squares at left in Figure 3, over 99% removal occurred in 8 min. For 10 g Fe_3O_4/L, circles

https://doi.org/10.1021/acsestwater.2c00242
ACS EST Water 2022, 2, 1584−1592

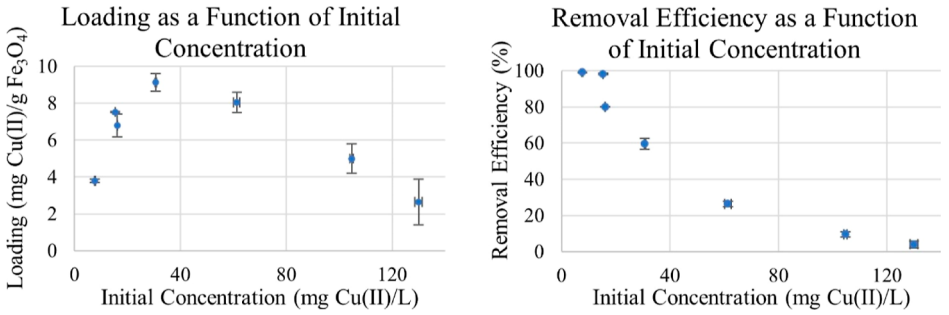

Figure 4. Copper loading values (left) and removal efficiencies (right) after 24 h with varying initial Cu(II) concentrations and an approximately constant dose of 2 g Fe_3O_4/L.

Table 2. Single-Stage Ion Removal

contaminant type	C_i (mg C/L)	C_f (mg C/L)	loading (mg C/g Fe_3O_4)	removal efficiency (%)
Cu(II)	107.0 ± 0.4	0.10 ± 0.01	5.34 ± 0.02	99.91 ± 0.01
Pb(II)	97.3 ± 3.5	0.11 ± 0.01	4.86 ± 0.17	99.91 ± 0.00
PO_4^{3-}	305.1 ± 0.6	99.75 ± 0.00	10.26 ± 0.21	67.31 ± 1.46
PO_4^{3-}	100.8	0.83	4.99	99.17
NO_3^-	104.3	96.51	0.39	7.47
mixed—NO_3^-	100.5	98.72	0.09	1.76
mixed—Pb(II)	167.9	0.09	8.39	99.95
mixed—Cu(II)	106.9 ± 0.0	0.26 ± 0.05	5.33 ± 0.00	99.70 ± 0.05
mixed—Pb(II)	95.8 ± 0.1	0.25 ± 0.04	4.77 ± 0.01	99.73 ± 0.04

Table 3. Two-Stage Copper Removal

stage	C_i (mg Cu(II)/L)	C_f (mg Cu(II)/L)	loading (mg Cu(II)/g Fe_3O_4)	removal efficiency (%)	cumulative removal (%)
1	104.0	0.25	5.18	99.76	
2	0.3	0.05	0.0084	78.95	99.95
1	104.0	0.33	5.18	99.68	
2	0.3	0.02	0.0129	93.13	99.98
1	104.0	0.18	5.19	99.83	
2	0.2	0.01	0.0070	92.88	99.99

and X's at left in Figure 3, 75% removal was achieved in 30 min and the overall removal was 84%. As expected, decreasing the dose resulted in lower contaminant removal. Increasing the agitation speed did not have a significant effect, where 400 rpm, circles at left in Figure 3, and 600 rpm, X's at left in Figure 3, data lay practically on top of each other.

Contaminant concentration was also explored, displayed at right in Figure 3. Experiments were conducted using 1 L of surrogate solution, dose of 20 g Fe_3O_4/L, and agitation speed of 400 rpm. For 200 mg Cu(II)/L, circles at right in Figure 3, 75% removal was achieved in 4 min with an overall removal of 89%, indicating the need for a higher dose or longer contact time to achieve complete Cu(II) removal. Over 99% removal was achieved in 8 min using 100 mg Cu/L, squares at right in Figure 3, and in 1 min using 50 mg Cu(II)/L, X's at right in Figure 3. Overall, rapid adsorption occurs in all tested contaminants, even at high concentrations, indicating short contact times and small reaction vessels can be used, depending on the volume of water being treated.

4.2. Contaminant Removal Experiments. *4.2.1. Loading Experiments.* Loading experiments were conducted to evaluate maximum loading capacity and removal efficiencies of Fe_3O_4 in surrogate solutions at varying Cu(II) concentrations and approximately constant doses of 2.0 g Fe_3O_4/L. Experiments were performed in triplicate and average values are displayed in Figure 4 with error bars representing standard deviation.

Loading data, presented at left in Figure 4, reveal that loading capacity increases until it hits a saturation point. Once the saturation point is reached, the limited number of available adsorption sites on the Fe_3O_4 are filled, leading to a decrease in loading capacity at higher initial concentrations observed at left in Figure 4. As displayed at right in Figure 4, near-complete removal occurs at low concentrations of Cu(II), but removal efficiency drops off quickly to around 60% at only 30 mg Cu(II)/L, indicating Fe_3O_4 saturation. At low doses of Fe_3O_4, saturation occurs quickly, with less than 10% removal at concentrations above 100 mg Cu(II)/L, but complete or near-complete removal is achieved at higher concentrations of Cu(II) with increased doses of Fe_3O_4. The increased adsorption behavior is demonstrated in Figures 1 and 3 and Table 3, where doses of up to 20 g Fe_3O_4/L and concentrations up to 200 mg Cu(II)/L achieved over 89% copper removal.

https://doi.org/10.1021/acsestwater.2c00242
ACS EST Water 2022, 2, 1584−1592

For economic and technical feasibility of using Fe_3O_4 in a CFMR system, increasing loading capacity may need to be considered for real-time, commercial operation, utilizing surface coatings and functionalizations, such as chitosan, silica, or EDTA.[6,7,14,29,31,38] Additional experiments investigating pH, temperature, and solution, or particle, conditioning will be conducted to create a more in-depth series of experiments for Fe_3O_4. Real water samples will also be collected and characterized for the contaminant content and then treated with Fe_3O_4 for comparison of removal efficiencies to surrogate solutions. Overall, future experimentation will build a comprehensive study of adsorption by bare Fe_3O_4 with supplemental data gathered for select modified particles and contaminants.

4.2.2. Single- and Two-Stage Ion Removal. Single- and two-stage ion removal data are displayed in Tables 2 and 3, respectively, where C_i and C_f represent the initial and final concentrations, respectively, in milligrams of contaminant per liter (mg C/L) and the loading and removal efficiency are calculated using eqs 1 and 2, respectively.

Single-stage ion removal experiments were performed to demonstrate that a high dose of Fe_3O_4 (20.0 g/L) can achieve complete or near-complete removal of contaminants from solution. Triplicate experiments were run on single contaminant experiments with Cu(II), Pb(II), 300 mg PO_4^{3-}/L, and the mixed Cu(II) and Pb(II) experiment, with averages and standard deviations presented in Table 2. Single experiments were run with PO_4^{3-}, NO_3^-, and mixed NO_3^- and Pb(II), where additional experiments are required to verify reproducibility of data.

Near-complete contaminant removal occurred in almost every case, achieving over 99% removal, except for nitrate. In the mixed metal case, though removal efficiencies for each metal were still high, slightly less Cu(II) and Pb(II) were removed from the solution compared to single metal experiments. As the experiments were performed under almost identical conditions, it is reasonable that less would be removed, as combined there was approximately 200 mg C/L in solution. For nitrate, many factors could explain the low removal, including solution pH and temperature, higher affinities for calcium and lead (both +2 cations) onto Fe_3O_4, or ion resonance structure; therefore, additional testing will be performed to determine the cause of low nitrate removal.

Table 2 displays exceptional removal efficiencies for most contaminants tested, but there are certain standards set by the Montana Department of Environmental Quality (DEQ) and the United States Environmental Protection Agency (EPA) for regulating the concentration of harmful contaminants to ensure a healthy quality of water. According to these standards, copper should be below 0.00285 mg/L, lead below 0.0006 mg/L, nitrate below 0.0001 mg/L, and phosphorus below 0.009 mg/L for aquatic life.[17,41] Though near-complete removal is achieved for Cu(II), Pb(II), and PO_4^{3-}, final concentrations fall short of the trace-level aquatic life standards set by the DEQ and EPA, indicating higher doses, longer contact times, or multiple stages are necessary to remove contaminants to these standards.

Two-stage experiments were performed to begin the investigation into contaminant removal using multiple stages on the same solution. Experiments used Cu(II) surrogate solutions, 20.0 g Fe_3O_4/L, and were run in triplicate, with data presented in Table 3. Cu(II) was chosen for initial scoping experiments, as it is the main focus of prior experimentation and the most prominent contaminant in the authors' location.[36] Near-complete removal occurred in all cases with only slight variation between experiments, displaying excellent experimental reproducibility.

Though, again, over 99% removal is achieved, final concentrations fall short of the trace-level aquatic life standards set by the DEQ and EPA. Therefore, additional multi-stage experiments are needed to determine the minimum number of stages required to reduce contaminants below DEQ and EPA aquatic life standards.

4.3. Cycling. Cycling was briefly explored to evaluate the reusability of bare Fe_3O_4 particles. One set of cycling experiments used fresh Fe_3O_4 after each cycle, circles in Figure 5, and the other used Fe_3O_4 that was stripped and regenerated after each cycle, triangles in Figure 5. The same solution was used for the entire experiment in both cases, and solution loss over the course of the experiments was assumed to be negligible.

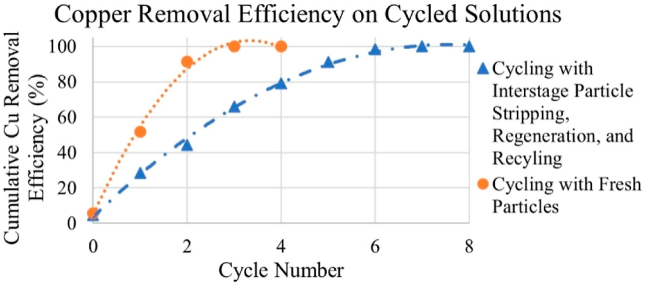

Figure 5. Cycling efficiencies for copper removal. Two experiments were performed using Fe_3O_4 particles, where one experiment used stripped and regenerated particles after each cycle (triangles) and the other used fresh particles after each cycle (circles). The lines connecting the points are for visual purposes only.

Cycling experiments where fresh Fe_3O_4 was added after each cycle reached near-complete removal of Cu(II) from the solution after four cycles, with initial and final concentrations of 51.11 and 0.035 mg Cu(II)/L, respectively. The solution containing stripped and regenerated particles took double that time, at eight cycles, for near-complete removal of Cu(II), with initial and final concentrations of 51.51 and 0.013 mg Cu(II)/L, respectively. Some particle loss occurred with the stripped and regenerated Fe_3O_4, ending the final cycle with 1.21 g Fe_3O_4/L. While the stripped and regenerated Fe_3O_4 pulled out more Cu(II) than the fresh Fe_3O_4, double the number of cycles was required. For economic considerations, a combination of fresh particles and stripped and regenerated particles may be best suited to maximize removal and minimize waste in a CFMR system.

Further investigation into cycling and the strip and regeneration process should be considered for future study. Investigating the optimal balance of fresh and stripped and regenerated particles will be considered for decreasing the required cycles to achieve near-complete or complete contaminant removal. Optimization of the strip and regeneration process for copper and specific procedures for other ions is essential for developing a cost-effective process. Additionally, determining what other contaminants can be stripped could increase particle reusability and recovery of reclaimable contaminants. Finally, studying strip solution cycling to attain a higher metal content for use in metal recovery processes can decrease waste production in the CFMR system, creating

https://doi.org/10.1021/acsestwater.2c00242
ACS EST Water 2022, 2, 1584−1592

Table 4. ANOVA and Fit Statistics

ANOVA for quadratic model						
source	sum of squares	df	mean square	*F*-value	*P*-value	
block	0.7482	1	0.7482			
model	27.80	5	5.56	5031.13	<0.0001	significant
A—pH	1.38	1	1.38	1247.43	<0.0001	
B—dose	16.11	1	16.11	14578.68	<0.0001	
AB	2.07	1	2.07	1871.89	<0.0001	
A^2	0.9061	1	0.9061	819.83	<0.0001	
B^2	10.90	1	10.90	9862.45	<0.0001	
residual	0.0055	5	0.0011			
lack of fit	0.0046	1	0.0046	19.56	0.0115	significant
pure error	0.0009	4	0.0002			
cor total	28.56	11				
			fit statistics			
std. dev.	0.0332			R^2	0.9998	
mean	9.33			adjusted R^2	0.9996	
C.V. %	0.3564			predicted R^2	0.9837	
				adeq precision	221.6938	

products from the metal-laden solutions rather than disposing them.

4.4. Design of Experiments. A statistical design of experiments was created using Design-Expert 12 to optimize the adsorption of Cu(II) onto Fe_3O_4. The design consisted of two numerical factors, pH and Fe_3O_4 dose, and one response, percent Cu(II) removed. The results of the 15 experiments were input into the Design-Expert 12 statistical design for analysis by the software. An automatic model selection using Akaike's information criterion estimates the quality of each model relative to other potential models and determines the terms to be kept in the model; in this case, all terms were kept, as seen in Table 4. A quadratic model with a square-root transform was chosen as the best model for the data. Once a model has been generated, an analysis of variance (ANOVA) presents statistical tests, where *p*-values less than 0.05 of the model and less than 0.1 of the variables suggest significance. Table 4 displays the ANOVA results, indicating the model and all factors are significant with *p*-values less than 0.0001. Further, fit statistics, displayed in Table 4, can aid in determining model quality. Differences in R^2 terms determine if the model fits the data and can accurately interpolate points. Agreement between R^2, adjusted R^2, and predicted R^2 suggests that the model fits the data. Predicted R^2 indicates that the model can predict responses for new variables. Additionally, adequate precision, which evaluates the signal-to-noise ratio, indicates a strong signal for model optimization. Overall, the ANOVA and fit statistics indicate the generated model is a good fit for the data.

In addition to ANOVA and fit statistics, diagnostics tools reveal supplementary information about trends, outliers, and influences on the model (Supporting Information, Text S2 and Figure S2). One diagnostic plot is the 3D Response Surface, a graphical representation of the model, displayed in Figure 6, with pH on the *y*-axis, dose on the *x*-axis, and % Cu removed on the vertical axis. Figure 6 suggests an acidic pH between 3 and 4.5 and doses above 14 g Fe_3O_4/L are optimal for Cu(II) removal.

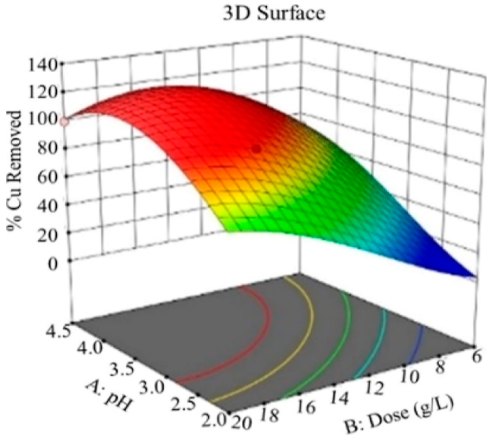

Figure 6. Diagnostic plot of the 3D response surface for the model of copper removal by magnetite, varying the pH and dose.

Six confirmation points were arbitrarily chosen from a list generated by Design-Expert 12 to evaluate the predictive capabilities of the model and statistically validate it. Table 5 presents the confirmation point data, where four of the six points fit within the 95% confidence intervals. One point was slightly lower, by less than 1%, and one was higher, by less than 5%, than the predicted intervals, italicized in Table 5. As only two points were marginally outside the ranges calculated by Design-Expert 12, it was concluded that the confirmation points indicate a good model with predictive capabilities.

Table 5. Design of Experiments Confirmation Points

confirmation point	95% PI low	data mean	95% PI high
1	*88.14*	*96.12*	*91.95*
2	98.07	98.93	101.84
3	97.74	98.51	101.84
4	*97.48*	*96.84*	*102.25*
5	87.93	90.87	92.06
6	87.89	89.56	92.26

https://doi.org/10.1021/acsestwater.2c00242
ACS EST Water 2022, 2, 1584−1592

5. CONCLUSIONS

Magnetite use as an adsorbent was examined for the removal of Cu(II), Pb(II), PO_4^{3-}, and NO_3^-. Kinetics experiments revealed a rapid initial adsorption rate and fit the PSO kinetic model, suggesting chemical adsorption is the rate-limiting step. At low doses of Fe_3O_4, material saturation was reached at low Cu(II) concentrations, indicating the need for increased doses of Fe_3O_4 for high contaminant concentrations. Single- and two-stage experiments confirmed the need for higher Fe_3O_4 doses at higher contaminant concentrations, removing over 99% of contaminant ions at initial concentrations of 100 mg/L with an increased dose of 20 g Fe_3O_4/L. The model generated by Design-Expert 12 suggests optimal conditions for sufficient Cu(II) removal in an acidic pH between 3 and 4.5 and doses above 14 g Fe_3O_4/L. Additional parameters, such as contact time, temperature, and multiple contaminants, should be considered in future studies to further refine the model. Overall, results from this study reveal that contaminant adsorption by magnetite may be a promising, economical, and simple solution for water pollution. Additionally, the process can be modified for a variety of applications, including environmental contamination and prevention of contaminant release from industrial wastewaters.

■ ASSOCIATED CONTENT

Supporting Information

The Supporting Information is available free of charge at https://pubs.acs.org/doi/10.1021/acsestwater.2c00242.

Magnetite SEM image description; magnetite SEM images; Design-Expert 12 Diagnostics Plot descriptions; and Design-Expert 12 Diagnostics Plots (PDF).

■ AUTHOR INFORMATION

Corresponding Author

Teagan J. Leitzke − *Materials Science Ph.D. Program, Montana Technological University, Butte, Montana 59701, United States;* orcid.org/0000-0002-5769-4926; Email: tleitzke@mtech.edu

Authors

J. Downey − *Materials Science Ph.D. Program, Montana Technological University, Butte, Montana 59701, United States; Metallurgical and Materials Engineering, Montana Technological University, Butte, Montana 59701, United States*

Richard M. LaDouceur − *Mechanical Engineering, Montana Technological University, Butte, Montana 59701, United States*

Daisy M. Margrave − *Materials Science and Engineering M.S. Program, Montana Technological University, Butte, Montana 59701, United States*

Grant C. Wallace − *Metallurgical and Materials Engineering, Montana Technological University, Butte, Montana 59701, United States*

David L. Hutchins − *Metallurgical and Materials Engineering, Montana Technological University, Butte, Montana 59701, United States*

Complete contact information is available at: https://pubs.acs.org/10.1021/acsestwater.2c00242

Author Contributions

CRediT Author Statement: **Teagan Leitzke:** data curation, formal analysis, investigation, methodology, software, validation, visualization, writing—original draft, writing—review and editing. **Jerome Downey:** conceptualization, funding acquisition, project administration, resources, supervision, writing—review and editing. **Richard LaDouceur:** methodology, formal analysis, writing—review and editing. **Daisy Margrave:** formal analysis. **Grant Wallace:** formal analysis, writing—review and editing. **David Hutchins:** conceptualization, methodology, writing—review and editing.

Notes

The authors declare no competing financial interest.

■ ACKNOWLEDGMENTS

This material is based upon work supported in part by the National Science Foundation EPSCoR Cooperative Agreement OIA-1757351. Any opinions, findings, and conclusions or recommendations expressed in this material are those of the author(s) and do not necessarily reflect the views of the National Science Foundation.

■ REFERENCES

(1) Jaishankar, M.; Tseten, T.; Anbalagan, N.; Mathew, B. B.; Beeregowda, K. N. Toxicity, mechanism and health effects of some heavy metals. *Interdiscip. Toxicol.* **2014**, *7*, 60−72.

(2) Tchounwou, P. B.; Yedjou, C. G.; Patlolla, A. K.; Sutton, D. J. Heavy Metal Toxicity and the Environment. *Molecular, Clinical and Environmental Toxicology. Experientia Supplementum* **2012**, *101*, 133−164.

(3) Vunain, E.; Mishra, A. K.; Mamba, B. B. Dendrimers, mesoporous silicas and chitosan-based nanosorbents for the removal of heavy-metal ions: a review. *Int. J. Biol. Macromol.* **2016**, *86*, 570−586.

(4) Besser, J. M.; Leib, K. J.. Toxicity of metals in water and sediment to aquatic biota. *Integrated investigations of environmental effects of historical mining in the Animas River watershed*: San Juan County, Colorado; Church, S. E., von Guerard, P., Eds.; *Finger, S.E.*; U.S. Geological Survey Professional Paper 1651, 2007; Vol. *2*, pp 837−849.

(5) El-Dib, F. I.; Mohamed, D. E.; El-Shamy, O. A. A.; Mishrif, M. R. Study the adsorption properties of magnetite nanoparticles in the presence of different synthesized surfactants for heavy metal ions removal. *Egypt. J. Pet.* **2020**, *29*, 1−7.

(6) Ghasemi, E.; Heydari, A.; Sillanpää, M. Superparamagnetic Fe_3O_4@EDTA nanoparticles as an efficient adsorbent for simultaneous removal of Ag(I), Hg(II), Mg(II), Zn(II), Pb(II), and Cd(II) from water and soil environmental samples. *Microchem. J.* **2017**, *131*, 51−56.

(7) Sarode, S.; Upadhyay, P.; Khosa, M. A.; Mak, T.; Shakir, A.; Song, S.; Ullah, A. Overview of wastewater treatment methods with special focus on biopolymer chitin-chitosan. *Int. J. Biol. Macromol.* **2019**, *121*, 1086−1100.

(8) Wang, J.; Tong, X.; Chen, Y.; Sun, T.; Liang, L.; Wang, C. Enhanced removal of Cr(III) in high salt organic wastewater by EDTA modified magnetic mesoporous silica. *Microporous Mesoporous Mater.* **2020**, *303*, 110262.

(9) Zwain, H. M.; Vakili, M.; Dahlan, I. Waste material adsorbents for zinc removal from wastewater: a comprehensive review. *Int. J. Chem. Eng.* **2014**, *2014*, 3479121.

(10) Anirudhan, T. S.; Noeline, B. F.; Manohar, D. M. Phosphate removal from wastewaters using a weak anion exchanger prepared from a lignocellulosic residue. *Environ. Sci. Technol.* **2006**, *40*, 2740−2745.

(11) Cho, D. W.; Song, B.; Kim, F. W.; Schwartz, B.-H.; Jeon, B.-H. Reduction of nitrate in groundwater by Fe(0)/magnetite nano-

particles entrapped in Ca-Alginate beads. *Water, Air, Soil Pollut.* **2015**, *226*, 206.
(12) Ebrahimi, S.; Roberts, D. J. Sustainable nitrate-contaminated water treatment using multi cycle ion-exchange/bioregeneration of nitrate selective resin. *J. Hazard. Mater.* **2013**, *262*, 539−544.
(13) Loganathan, P.; Vigneswaran, S.; Kandasamy, J.; Bolan, N. S. Removal and recovery of phosphate from water using sorption. *Crit. Rev. Environ. Sci. Technol.* **2014**, *44*, 847−907.
(14) Morsi, R. E.; Al-Sabagh, A. M.; Moustafa, Y. M.; ElKholy, S. G.; Sayed, M. S. Polythiophene modified chitosan/magnetite nanocomposites for heavy metals and selective mercury removal. *Egypt. J. Pet.* **2018**, *27*, 1077−1085.
(15) Malhotra, N.; Ger, T.-R.; Uapipatanakul, B.; Huang, J.-C.; Chen, K. H.-C.; Hsiao, C.-D. Review of copper and copper nanoparticle toxicity in fish. *Nanomaterials* **2020**, *10*, 1126.
(16) O'Brien, E. *Biologists Suspect Mine Waste in Clark Fork Fish Kill*; Montana Public Radio, 2019. (accessed April 18, 2022) https://www.mtpr.org/post/biologists-suspect-mine-waste-clark-fork-fish-kill .
(17) Montana Department of Environmental Quality. *Planning Prevention and Assistance Division, Water Quality Planning Bureau, Water Quality Standards Section*; U.S. Environmental Protection Agency, 2012. (accessed July 03, 2022), Department Circular DEQ-7. https://www.epa.gov/sites/production/files/2014-12/documents/mtdeq7.pdf .
(18) U.S. Geological Survey. *National Water Information System: Map View*; USGS, 2020. (accessed April 18, 2022). https://maps.waterdata.usgs.gov/mapper
(19) Bombuwala Dewage, N.; Liyanage, A. S.; Pittman, C. U., Jr.; Mohan, D.; Mlsna, T. Fast nitrate and fluoride adsorption and magnetic separation from water on α-Fe_2O_3 and Fe_3O_4 dispersed on Douglas fir biochar. *Bioresour. Technol.* **2018**, *263*, 258−265.
(20) Kim, Y.-S.; Lee, Y.-H.; An, B.; Choi, S.-A.; Park, J.-H.; Jurng, J.-S.; Lee, S.-H.; Choi, J.-W. Simultaneous removal of phosphate and nitrate in wastewater using high-capacity anion-exchange resin. *Water, Air, Soil Pollut.* **2012**, *223*, 5959−5966.
(21) U.S. Environmental Protection Agency. *Nutrient Indicators Dataset*; EPA, 2020. (accessed March 08 2022). https://www.epa.gov/nutrient-policy-data/nutrient-indicators-dataset.
(22) Schons, M. Superfund. *National Geographic*, 2011. (accessed March 18, 2022). https://www.nationalgeographic.org/article/superfund/.
(23) Mao, M.; Yan, T.; Shen, J.; Zhang, J.; Zhang, D. Selective Capacitive Removal of Heavy Metal Ions from Wastewater over Lewis Base Sites of S-Doped Fe−N−C Cathodes *via* an Electro-Adsorption Process. *Environ. Sci. Technol.* **2021**, *55*, 7665−7673.
(24) Mao, M.; Yan, T.; Chen, G.; Zhang, J.; Shi, L.; Zhang, D. Selective Capacitive Removal of Pb^{2+} from Wastewater over Redox-Active Electrodes. *Environ. Sci. Technol.* **2021**, *55*, 730−737.
(25) Ahmed, M. A.; Ali, S. M.; El-Dek, S. I.; Galal, A. Magnetite-hematite nanoparticles prepared by green methods for heavy metal ions removal from water. *Mater. Sci. Eng., B* **2013**, *178*, 744−751.
(26) Rajput, S.; Pittman, C. U., Jr.; Mohan, D. Magnetic magnetite (Fe_3O_4) nanoparticle synthesis and applications for lead (Pb^{2+}) and chromium (Cr^{6+}) removal from water. *J. Colloid Interface Sci.* **2016**, *468*, 334−346.
(27) Hutchins, D. L.; Downey, J. P. Effective separation of magnetite nanoparticles within an industrial-scale pipeline reactor. *Sep. Sci. Technol.* **2019**, *55*, 2822−2829.
(28) Laurent, S.; Forge, D.; Port, M.; Roch, A.; Robic, C.; Vander Elst, L.; Muller, R. N. Magnetic iron oxide nanoparticles: Synthesis, stabilization, vectorization, physicochemical characterizations and biological applications. *Chem. Rev.* **2008**, *108*, 2064−2110.
(29) Leitzke, T.; Downey, J. P.; Hutchins, D.; St. Clair, St.B. Continuous Flow Process for Removal and Recovery of Water Contaminants with Magnetic Nanocomposites. In *Nanocomposites VI: Nanoscience and Nanotechnology in Advanced Composites*; Srivatsan, T. S., Gupta, M., Eds., 2019, pp 155−164.
(30) Popescu, C. R.; Andronescu, E.; Vasile, B. S. Recent Advances in Magnetite Nanoparticle Functionalization for Nanomedicine. *Nanomaterials* **2019**, *9*, 1791.
(31) Wang, J.; Zheng, S.; Shao, Y.; Liu, J.; Xu, Z.; Zhu, D. Amino-functionalized Fe_3O_4@SiO_2 core-shell magnetic nanomaterial as a novel adsorbent for aqueous heavy metals removal. *J. Colloid Interface Sci.* **2010**, *349*, 293−299.
(32) Liang, X.; Lin, X.; Wei, G.; Ma, L.; He, H.; Santos-Carballal, D.; Zhu, J.; Zhu, R.; De Leeuw, N. H. Competitive adsorption geometries for the arsenate As(V) and phosphate P(V) oxyanions on magnetite surfaces: Experiments and theory. *Am. Mineral.* **2021**, *106*, 374−388.
(33) Zhang, J.; Lin, S.; Han, M.; Su, Q.; Xia, L.; Hui, Z. Adsorption properties of magnetic magnetite nanoparticle for coexistent Cr(VI) and Cu(II) in mixed solution. *Water* **2020**, *12*, 446.
(34) Cheng, Z.; Tan, A. L. K.; Tao, Y.; Shan, D.; Ting, K. E.; Yin, X. J. Synthesis and characterization of iron oxide nanoparticles and applications in the removal of heavy metals from industrial wastewater. *Int. J. Photoenergy* **2012**, *2012*, 6082981.
(35) Kalpakli, Y. Removal of Cu(II) from aqueous solutions using magnetite: A kinetic, equilibrium study. *Adv. Environ. Res.* **2015**, *4*, 119−133.
(36) Hutchins, D. *Continuous Flow Process for Recovery of Metal Contaminants from Industrial Wastewaters with Magnetic Nanocomposites*; Ph.D. Dissertation, Montana Technological University: Butte, MT, 2018.
(37) Crittenden, J. C.; Trussell, R. R.; Hand, D. W.; Howe, K. J. Tchobanoglous. *G. Water Treatment: Principles and Design*, 3rd ed.; John Wiley & Sons, Inc.: Hoboken, NJ, 2012.
(38) Liu, Y.; Chen, M.; Yongmei, Y. Study on the adsorption of Cu(II) by EDTA functionalized Fe_3O_4 magnetic nano-particles. *Chem. Eng. J.* **2013**, *218*, 46−54.
(39) Cho, D.-W.; Jeon, B.-H.; Chon, C.-M.; Kim, Y.; Schwartz, F. W.; Lee, E.-S.; Song, H. A novel chitosan/clay/magnetite composite for adsorption of Cu(II) and As(V). *Chem. Eng. J.* **2012**, *200*−*202*, 654−662.
(40) Keyvani, F.; Rahpeima, S.; Javanbakht, V. Synthesis of EDTA-modified magnetic activated carbon nanocomposite for removal of permanganate from aqueous solutions. *Solid State Sci.* **20182018**, *83*, 31−42.
(41) Montana Department of Environmental Quality. Department Circular DEQ-12A Montana Base Numeric Nutrient Standards; Montana Department of Environmental Quality, 2014. (accessed March 07, 2022). https://deq.mt.gov/files/Water/WQPB/Standards/PDF/NutrientRules/CircularDEQ12A-July2014-FINAL.pdf.

https://doi.org/10.1021/acsestwater.2c00242
ACS EST Water 2022, 2, 1584−1592